iScience

CellPress
OPEN ACCESS

Article

Lack of xanthine dehydrogenase leads to a remarkable renal decline in a novel hypouricemic rat model

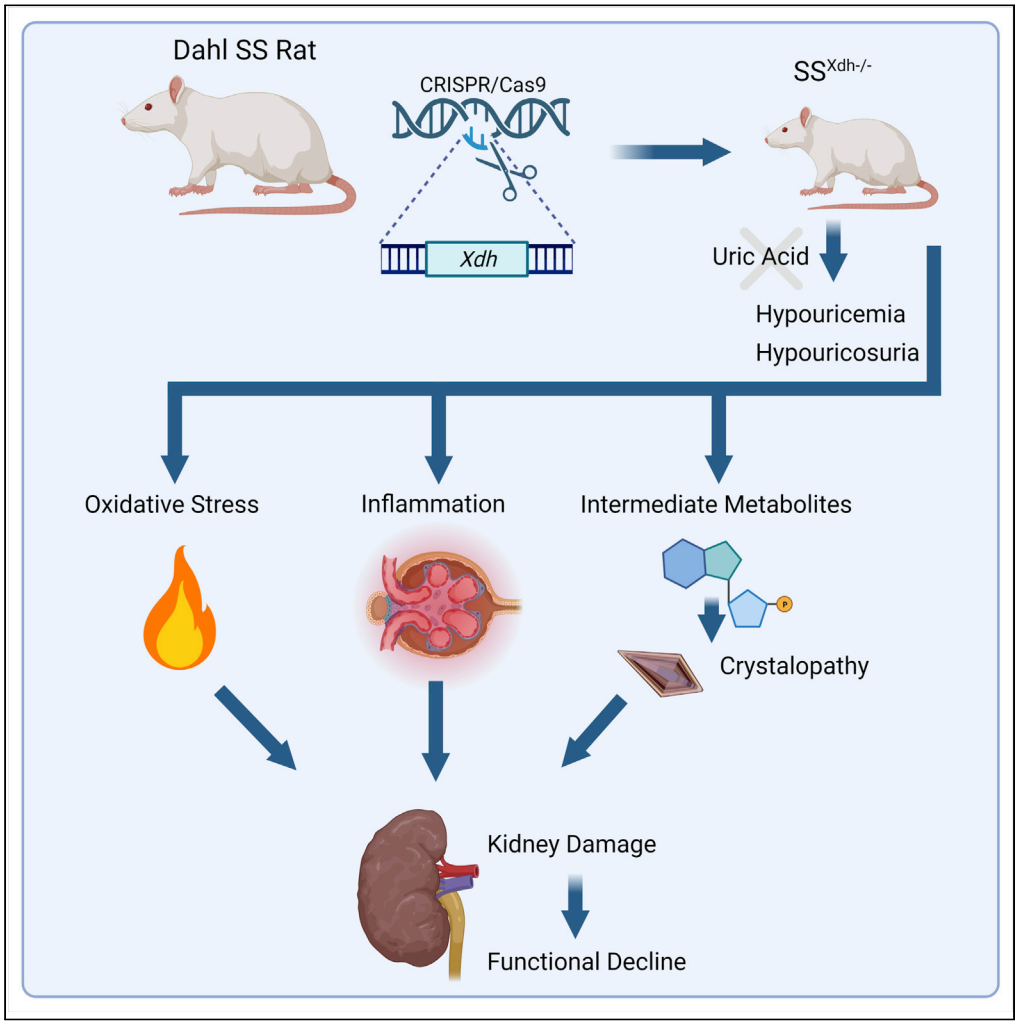

Lashodya V. Dissanayake, Adrian Zietara, Vladislav Levchenko, ..., Melinda R. Dwinell, Oleg Palygin, Alexander Staruschenko

staruschenko@usf.edu

Highlights

A novel rat model of hypouricemia was created by the gene ablation of the *Xdh* gene

The $SS^{Xdh-/-}$ rat showed a failure to thrive, kidney injury, and functional decline

Multi-omics revealed increased inflammation and oxidative stress in $SS^{Xdh-/-}$ rats

Dissanayake et al., iScience *25*, 104887
September 16, 2022
https://doi.org/10.1016/j.isci.2022.104887

iScience

CellPress
OPEN ACCESS

Article

Lack of xanthine dehydrogenase leads to a remarkable renal decline in a novel hypouricemic rat model

Lashodya V. Dissanayake,[1,2] Adrian Zietara,[1,2] Vladislav Levchenko,[1] Denisha R. Spires,[3] Mariana Burgos Angulo,[1] Ashraf El-Meanawy,[4] Aron M. Geurts,[2] Melinda R. Dwinell,[2] Oleg Palygin,[5,6] and Alexander Staruschenko[1,7,8,9,*]

SUMMARY

Uric acid (UA) is the final metabolite in purine catabolism in humans. Previous studies have shown that the dysregulation of UA homeostasis is detrimental to cardiovascular and kidney health. The *Xdh* gene encodes for the Xanthine Oxidoreductase enzyme group, responsible for producing UA. To explore how hypouricemia can lead to kidney damage, we created a rat model with the genetic ablation of the *Xdh* gene on the Dahl salt-sensitive rat background ($SS^{Xdh-/-}$). $SS^{Xdh-/-}$ rats lacked UA and exhibited impairment in growth and survival. This model showed severe kidney injury with increased interstitial fibrosis, glomerular damage, crystal formation, and an inability to control electrolyte balance. Using a multi-omics approach, we highlighted that lack of *Xdh* leads to increased oxidative stress, renal cell proliferation, and inflammation. Our data reveal that the absence of *Xdh* leads to kidney damage and functional decline by the accumulation of purine metabolites in the kidney and increased oxidative stress.

INTRODUCTION

Uric acid (UA), the end-product of purine catabolism in humans, acts as a potent antioxidant in circulation by scavenging free radicals (Ames et al., 1981). However, UA can also be considered a conditional pro-oxidant when UA is catalyzed by Xanthine Oxidase (XO), producing reactive oxygen species (ROS). UA can be produced by both XO and Xanthine Dehydrogenase (XDH), and together these enzymes are known as Xanthine Oxidoreductase (XOR). The XOR proteins are encoded by the gene *XDH*. Both increased (hyperuricemia) and decreased (hypouricemia) serum UA levels are associated with all-cause mortality in patients with chronic kidney disease (CKD), as well as with the risk of future kidney function decline in healthy men (Kanda et al., 2015; Suliman et al., 2006). Numerous studies have shown that hyperuricemia can lead to cardiovascular disease, hypertension, and CKD, and the control of UA production by XDH inhibitors can be effective in managing these conditions (Cappola et al., 2001; Feig et al., 2008; Johnson et al., 2018; Lee et al., 2019; Shirakura et al., 2016; Verdecchia et al., 2000). Although there have been challenges in translating this knowledge to clinical practice, the mechanisms behind the pathogenesis of hyperuricemia are partially understood. Despite its apparent association with poor patient outcomes, hypouricemia has been far less studied than hyperuricemia, which may be owing to its lower prevalence (0.2-0.58% in the general population (Kuwabara et al., 2017; Son et al., 2016)).

Clinical conditions presenting with hypouricemia can be classified as disorders of decreased UA production or increased UA urinary excretion (hyperuricosuria) (Pineda et al., 2019). In both categories, there are inherited conditions (hereditary xanthinuria, purine nucleoside phosphorylase deficiency, hereditary renal hypouricemia types 1 & 2 (RHUC1 & 2)) as well as acquired disorders (overcorrection by UA-lowering therapy, liver disease (Michelis et al., 1974), malnutrition, Fanconi syndrome (Izzedine et al., 2003), diabetes mellitus, and so forth) resulting in hypouricemia. Although most clinical cases of hypouricemia present asymptomatically, some complications such as acute kidney injury (AKI) (Ichida et al., 2004; Ishikawa et al., 1990; Ohta et al., 2004), nephrolithiasis, and posterior reversible encephalopathy syndrome have been reported (Fujinaga et al., 2013). A mouse model of hyperuricosuria showed UA crystals and inflammasome activation with exercise-induced AKI (Hosoya et al., 2022).

[1]Department of Molecular Pharmacology & Physiology, Morsani College of Medicine, University of South Florida, 560 Channelside Dr., Tampa, FL 33602, USA

[2]Department of Physiology, Medical College of Wisconsin, Milwaukee, WI 53226, USA

[3]Department of Physiology, Medical College of Georgia, Augusta University, Augusta, GA 30912, USA

[4]Division of Nephrology, Department of Medicine, Medical College of Wisconsin, Milwaukee, WI 53226, USA

[5]Department of Medicine, Division of Nephrology, Medical University of South Carolina, Charleston, SC 29425, USA

[6]Department of Regenerative Medicine and Cell Biology, Medical University of South Carolina, Charleston, SC 29425, USA

[7]Hypertension and Kidney Research Center, University of South Florida, Tampa, FL 33602, USA

[8]James A. Haley Veterans' Hospital, Tampa, FL 33612, USA

[9]Lead contact

*Correspondence: staruschenko@usf.edu

https://doi.org/10.1016/j.isci.2022.104887

There are several mouse models of decreased UA production created from a knockout (KO) of the *Xdh* gene (Ohtsubo et al., 2004, 2009; Vorbach et al., 2002). These models showed severe kidney damage but had extremely low survival probability, which is problematic for chronic physiological studies (Ohtsubo et al., 2004, 2009; Vorbach et al., 2002). To our knowledge, there are no hypertensive rodent models of hypouricemia. Furthermore, it has been shown that renal XOR activity increases with the increase in salt intake in Dahl salt-sensitive (SS) but not salt-resistant rats (Laakso et al., 1998). It was also reported that long-term hyperuricemia could induce salt sensitivity in salt-resistant Sprague-Dawley rats (Watanabe et al., 2002). To gain a better understanding of the role of UA in the progression of kidney injury in a SS model, we created a KO of *Xdh* in the Dahl SS rat background. Using this model, we tested the hypothesis that the absence of UA (a major antioxidant) leads to kidney damage and functional decline by the accumulation of purine metabolites in the kidney and increased oxidative stress.

Through the utilization of a novel genetic model, phenotyping analyses, and multi-omics analyses, we were able to uncover mechanisms of UA dysregulation leading to impairment in renal structure and function.

RESULTS

Xdh deletion results in hypouricemia and a failure to thrive

The *Xdh* knockout ($SS^{Xdh-/-}$) model was created using CRISPR/Cas9 gene-editing resulting in a 7 base pair deletion in exon 4 of the *Xdh* gene on the Dahl SS rat background (Figure 1A), as validated by DNA sequencing. Western blotting with kidney cortex tissue of 6-week-old wild-type ($SS^{Xdh+/+}$), heterozygous ($SS^{Xdh+/-}$), and $SS^{Xdh-/-}$ rats showed that compared to the $SS^{Xdh+/+}$, $SS^{Xdh+/-}$ had decreased levels of the Xdh protein and $SS^{Xdh-/-}$ lacked the protein altogether (Figure 1B). Immunohistochemistry reiterated these results (Figure 1C), verifying the success of the KO. The homozygous rats demonstrated a lower survival probability (overall ~70%, male –78%, female – 64%) within the first 6 weeks of life compared to their littermates (Figures 1D and S1*A*). They also had significantly lower total body weights (TBW) than their littermate $SS^{Xdh+/+}$ and $SS^{Xdh+/-}$ rats, indicating a failure to thrive (Figures 1E and S1 *B*). On a gross anatomical level, the $SS^{Xdh-/-}$ rats lacked visceral adipose tissue in the abdominal cavity and surrounding organs. The *Xdh* KO also had significantly lower kidney weights, higher kidney weight/TBW, and higher heart weight/TBW ratios (Figures 1F–H and S1 *B*). As *Xdh* encodes for the XOR enzyme group that produces Uric acid (UA), we found an undetectable level of plasma UA in $SS^{Xdh-/-}$ rats (Figures 1I and S1 *B*) and only marginal urinary excretion (Figures 1J and S1 *B*) compared to the $SS^{Xdh+/+}$ and $SS^{Xdh+/-}$ littermates, which functionally confirmed the KO.

Lack of Xdh leads to kidney damage and functional decline

In examining the effects of the *Xdh* KO on kidney morphology and function, we found that $SS^{Xdh-/-}$ rats displayed kidney dysplasia with cysts as well as less differentiation between the cortical and medullary areas (Figure 2A). Additionally, $SS^{Xdh-/-}$ rats had significantly increased levels of interstitial fibrosis (Figures 2B and S1*C*). Further renal damage was localized to both glomeruli and tubules (Figures 2C and 2D). The homozygotic kidney cortices were mostly filled with fibrotic tissue, with only limited areas of tubules preserved (Figure 2C). The remaining tubules were dilated and damaged, which was confirmed by increased expression of kidney injury molecule-1 (Kim-1) (Figure 2D). Kim-1 is a marker of kidney damage in proximal tubule epithelial cells (Gardiner et al., 2012). Isolated glomeruli from $SS^{Xdh-/-}$ rats were significantly smaller compared to $SS^{Xdh+/+}$ glomeruli (Figure 2E). Additionally, we observed crystals throughout the kidney in $SS^{Xdh-/-}$ rats, which were not present in $SS^{Xdh+/+}$ kidneys (Figure 2F). Scoring of glomerular damage revealed a higher cumulative injury score in $SS^{Xdh-/-}$ vs $SS^{Xdh+/+}$ rats (Figure 2G). Glomeruli of the homozygous KO had fibrosis in and around the renal capsule, and some had a collapsing glomerular tuft.

The $SS^{Xdh-/-}$ rats exhibited a dramatic decline in kidney function with increased diuresis (Figure 2H) and increased plasma creatinine, which indirectly indicates an impaired glomerular filtration rate. (Figure 2I) However, there was no difference in albumin excretion in the homozygotes compared to wild-type littermates (Figure 2J). In the $SS^{Xdh-/-}$ rats, plasma Na^+ was significantly elevated compared to wild-type and heterozygous littermates, whereas Cl^- was significantly elevated compared to the wild-types (Table 1).

Because of the failure to thrive and kidney phenotypes we observed, we proceeded to test the urine excretion of aminoacids to detect signs of inborn errors of metabolism. In the $SS^{Xdh-/-}$ rat urine glutamine, citrulline, alanine, alpha-aminoadipic-acid, cystathionine 1, and total cysteine levels were significantly increased

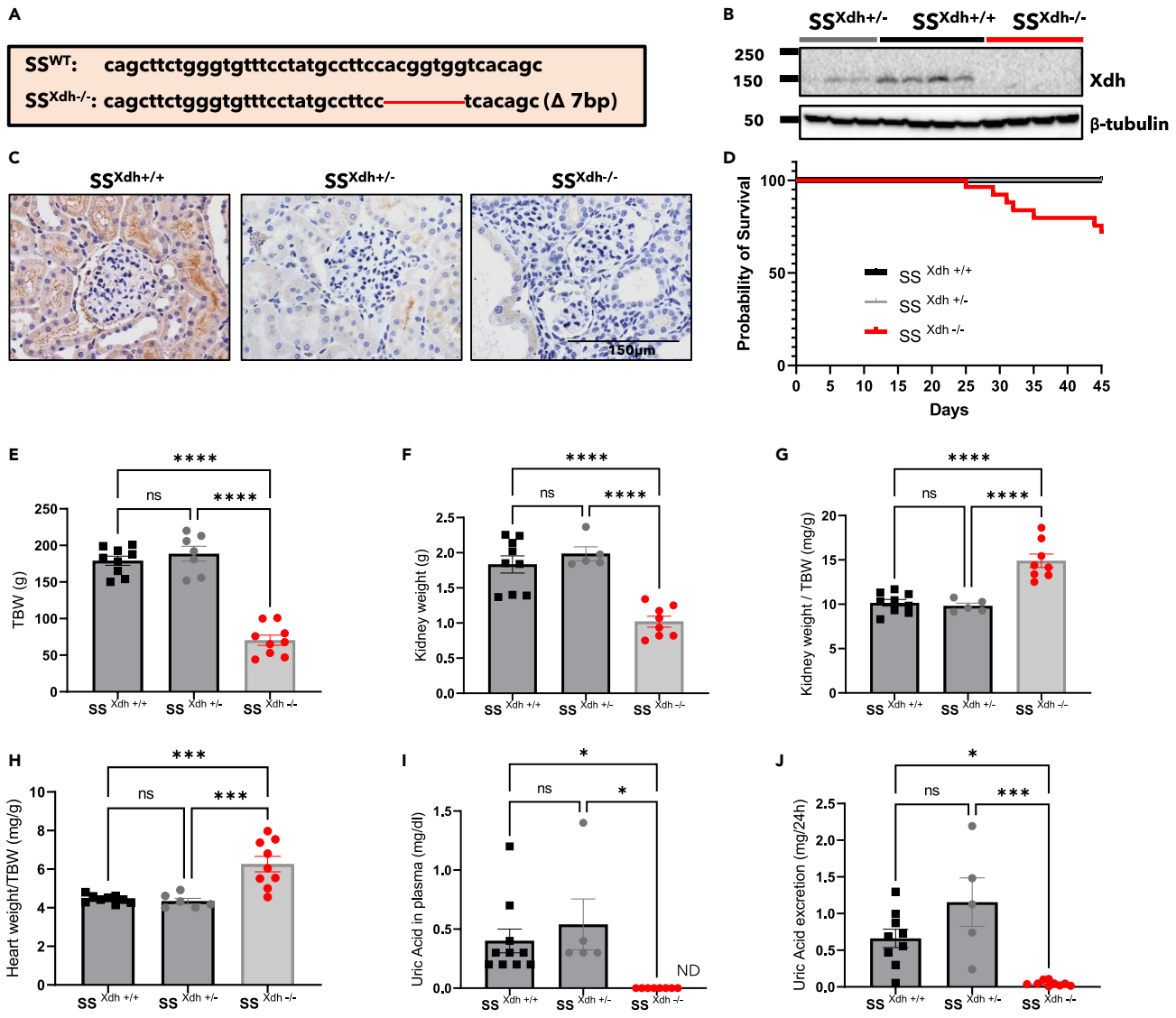

Figure 1. The Novel rat model of Xdh knockout in Dahl SS background

(A) Schematic showing the location of the deletion in the *Xdh* gene on rat chromosome 6.

(B) Western blotting analysis of Xdh expression in the kidney cortex of the $SS^{Xdh+/-}$, $SS^{Xdh+/+}$, and $SS^{Xdh-/-}$ rats (Each band = one rat).

(C) Representative images of immunostaining of Xdh protein in the kidneys of the $SS^{Xdh+/+}$, $SS^{Xdh+/-}$, and $SS^{Xdh-/-}$ rats (N = 4 per group).

(D–J) Survival probability of the $SS^{Xdh+/+}$ (N = 37), $SS^{Xdh+/-}$ (N = 57), and $SS^{Xdh-/-}$ (N = 28) rats in the first 6 weeks of their lives (For separate analyses on male and female survival see Figure S1A). (E) Total Body Weight (TBW), (F) Sum weight of both kidneys (G) Sum weight of kidneys/TBW ratio (H) Heart weight/TBW ratio, (I) Uricemia and (J) Uricosuria of the $SS^{Xdh+/+}$, $SS^{Xdh+/-}$, and $SS^{Xdh-/-}$ male rats (For female see Figure S1B). All data are from male 6-week-old rats except for Figure 1D which includes both males and females. ND = Not Detected (below the level of detection), in cases of ND, the lowest possible value of detection was used for statistical analyses. For E-J, N = the number of shapes; NS- not significant, * ≤0.05, ** ≤0.01, *** ≤0.001, **** ≤0.0001. Data are represented as mean ± SEM.

(Table 2). Arginine, sarcosine, gamma-amino-N-butyric-acid (GABA), beta-aminoisobutyric-acid, and total homocysteine excretion were significantly decreased (Table 2).

Xdh deletion is associated with significant differential expression of genes and metabolites

To determine whether knocking out *Xdh* can cause a differentially expressed gene profile, we conducted mRNA sequencing analysis using kidney cortex tissue of the $SS^{Xdh-/-}$ rats in comparison with $SS^{Xdh+/-}$ and $SS^{Xdh+/+}$ rats. We observed clear differences with hierarchical clustering in the gene expression profiles

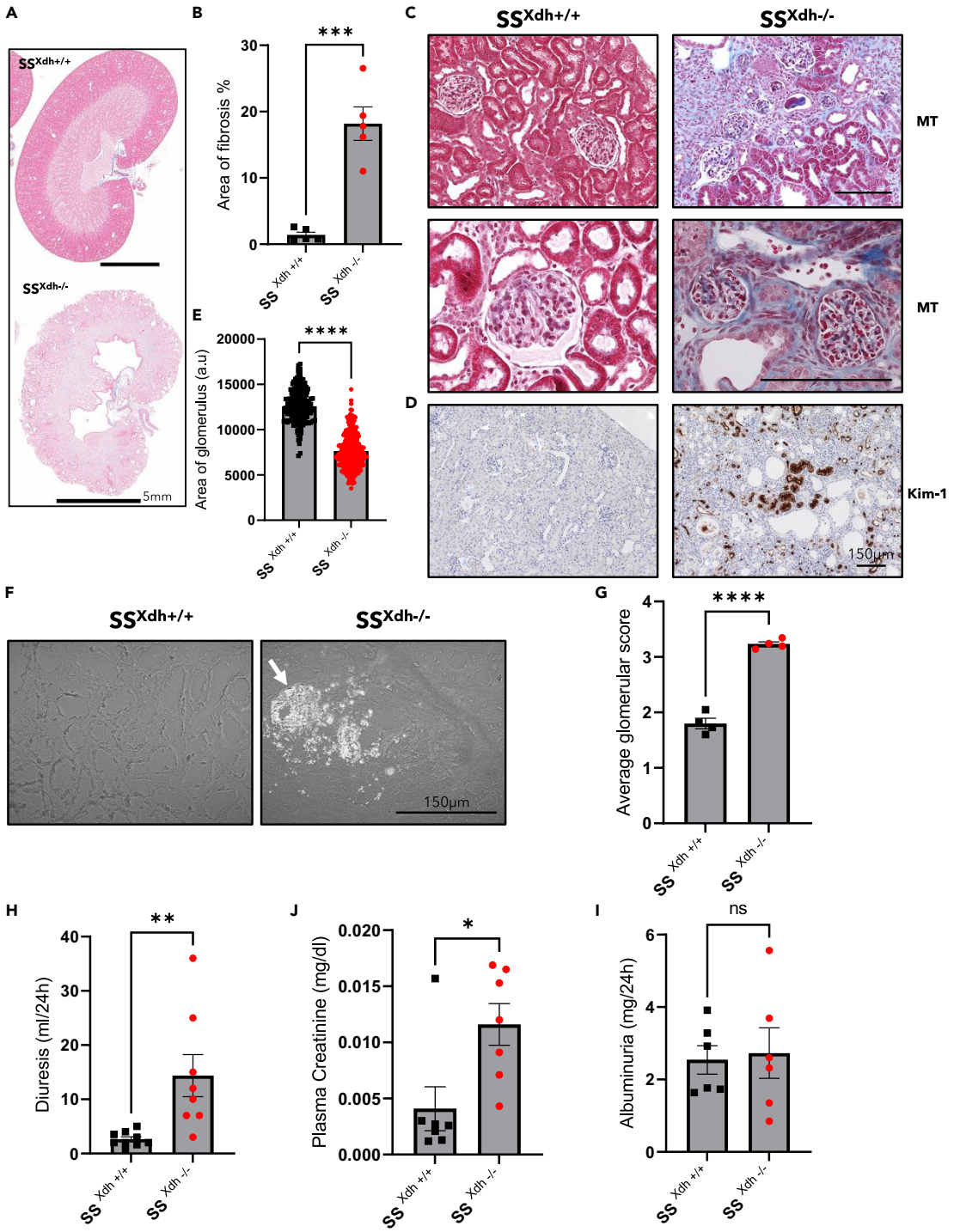

Figure 2. Kidney damage and functional decline in $SS^{Xdh-/-}$ rats

(A) Representative kidney sections of $SS^{Xdh+/+}$ and $SS^{Xdh-/-}$ rats stained with Masson's trichrome (MT) showing damage (blue-connective tissue, N = 5 per group).

(B) Quantification of percentage area of fibrosis in $SS^{Xdh+/+}$ and $SS^{Xdh-/-}$ rat kidneys (For female data relating to A & B, see Figure S1C).

(C) Representative kidney tissue sections showing the state of glomeruli and tubules in $SS^{Xdh+/+}$ and $SS^{Xdh-/-}$ rats stained in MT.

(D) Representative images of kidney sections stained in Kim-1 staining (brown) (N = 5 per group).

(E) Size of glomeruli quantified using isolated glomeruli from $SS^{Xdh+/+}$ (N = 3, n = 173) and $SS^{Xdh-/-}$ (N = 3, n = 270) rat kidneys (a.u-arbitrary units).

(F) Representative images of crystals in the kidney cortex under cross-polarized light. Shown in grayscale for clarity.

Figure 2. *Continued*

(G) Glomerular scores (0-4, 0 = no damage) based on scores assigned by an observer blinded to the study ($SS^{Xdh+/+}$ (N = 4, n = 902) and $SS^{Xdh-/-}$ (N = 4, n = 836)).

(H–J) Urinary output in 24 h, (I) Plasma creatinine and (J) Albumin excretion amount in 24 h of $SS^{Xdh+/+}$ and $SS^{Xdh-/-}$ rats. All data are from male 6-week-old rats. For B, E, G-I, N = the number of shapes; NS- not significant * ≤0.05, ** ≤0.01, *** ≤0.001, **** ≤0.0001. Data are represented as mean ± SEM.

(Figure 3A). From the pairwise approach of comparison, 4,940 and 4,926 genes were differentially expressed in homozygotic kidneys compared to wild-type and heterozygotic kidneys, respectively. Among these, 4,618 genes were differentially expressed in both comparisons. Interestingly only one gene (*Gns*/N-acetylglucosamine-6-sulfatase) was differentially expressed in heterozygotic kidneys compared to wild-type kidneys.

Similarly, we analyzed the kidney cortex tissue of $SS^{Xdh-/-}$ rats in comparison with $SS^{Xdh+/+}$ rats to profile the metabolomic differences using the untargeted approach. 2253 metabolites were identified as significantly differentially expressed. Hierarchical clustering of metabolites identified through negative HILIC mode is represented in Figure 3B.

Significant changes in energy metabolism, oxidative stress, and renal cell structure

Using Ingenuity Pathway Analysis (IPA), we assessed relationships, mechanisms, and functions to determine dysregulated critical pathways in our KO model. Purine catabolism, the target pathway of the KO, showed an accumulation of metabolites upstream of *Xdh*, including xanthosine and adenine (Figure 4A). The top canonical pathways that were suggested to be significantly changing in the $SS^{Xdh-/-}$ vs $SS^{Xdh+/+}$ rats were separately identified for each omics dataset. 51 different pathways were recognized as overlapping between transcriptomic and metabolomic analyses (Table S1). They strongly suggest the disruption of energy production and an increase of oxidative stress in the KO (Figures 4B and Table S1). Additionally, gene/metabolite lists for toxicity, upstream regulators, and disease/biological functions were generated (Tables S2–S10). The toxicity list based on RNA seq (Table S2) revealed a strong association with oxidative stress (-log(p-value) 4.79) and related functions (glutathione depletion, hypoxia-inducible factor/HIF signaling, long-term renal injury antioxidant/pro-oxidant response panels and NRF-2 mediated oxidative stress response). Additionally, the generation of ROS as a function was upregulated (Z-score 1.85, overlap p-value 3.11E-07).

Considering the striking kidney damage phenotype of the hypouricemic rats, we explored the related mechanisms and biological functions using the omics data. Increases in cell proliferation in the kidney are indicative of ongoing renal damage (Gewin et al., 2017; Priante et al., 2019). RNA sequencing data showed that the proliferation of kidney cells was upregulated (Table S2) and genes causally affecting the process were also identified as upregulated in $SS^{Xdh-/-}$ rat kidneys (Figures 4C and Table S3). Among these were genes encoding growth factors (*Mst1*, *Angpt2*, *Pdgfb*, *Tgfβ1*), cytokines (*Ccl21*), G protein-coupled receptors (*Cxcr3*), kinases (*Pdgfrb*, *Cdkn1a*), and transcriptional factors (*Stat3*) (Figure 4C). Furthermore, multiple genes that can affect renal ion transport were detected to be significantly changing in the KO homozygous rat kidneys (Table S8).

Transcriptomics revealed an increased inflammatory response

Pathway analysis using transcriptomics data showed the inflammatory response to be the most upregulated disease process based on the *Z* score (*Z* score 5.664, overlap p-value 1.05E-37). 144 different genes had measurement direction consistency (upregulated genes that are known to be increasing

Table 1. Plasma electrolyte concentrations

Plasma electrolyte (mM)	$SS^{Xdh+/+}$ *	$SS^{Xdh+/-}$ #	$SS^{Xdh-/-}$
K^+	4.4 ± 0.3 (N = 10)	3.9 ± 0.5 (N = 7)	4.8 ± 0.6 (N = 9)#
Na^+	136 ± 2 (N = 10)	138 ± 17 (N = 7)	150 ± 20 (N = 9) ***###
Ca^{2+}	1.19 ± 0.04 (N = 10)	1.19 ± 0.15 (N = 7)	1.11 ± 0.17 (N = 9)
Cl^-	105 ± 2 (N = 10)	105 ± 13 (N = 7)	113 ± 15 (N = 9) *

p-value: * Comparison with $SS^{Xdh+/+}$. # Comparison with $SS^{Xdh+/-}$ (* or# ≤0.05, ** or## ≤0.01, *** or### ≤0.001). Data are represented as mean ± SEM.

Table 2. Aminoaciduria

Amino acid excreted in 24 h (μmol/24h)	$SS^{Xdh+/+}$	$SS^{Xdh-/-}$
Arginine	1.04 ± 0.22	0.36 ± 0.08 *
Carnosine	0.027 ± 0.004	ND
Glutamine	0.48 ± 0.11	2.37 ± 0.5 *
Sarcosine	0.62 ± 0.10	0.12 ± 0.05 **
Citrulline	0.15 ± 0.03	1.99 ± 0.56 *
Alanine	1.84 ± 0.29	4.39 ± 0.86 *
gamma-Amino-N-butyric-acid	0.71 ± 0.14	0.20 ± 0.07 *
alpha-Aminoadipic-acid	0.010 ± 0.002	0.046 ± 0.011 *
beta-Aminoisobutyric-acid	0.072 ± 0.014	0.006 ± 0.001 **
Cystathionine 1	0.003 ± 0.001	0.040 ± 0.009 **
Total Cysteine	0.028 ± 0.003	0.094 ± 0.021 *
Total Homocysteine	0.051 ± 0.01	0.009 ± 0.002 **
Phenylalanine	0.314 ± 0.062	0.221 ± 0.042

p-value: * Comparison with $SS^{Xdh+/+}$. (* ≤0.05, ** ≤0.01, ND – not detected). Data are represented as mean ± SEM.

inflammation and downregulated genes that are known to be inhibiting inflammation) with an increased inflammatory response (Table S9). The inflammasome pathway is a cascade of protein complexes that activates pro-inflammatory molecules and is activated by ROS and mitochondrial dysfunction (Harijith et al., 2014; Mishra et al., 2021). The inflammasome signaling pathway was upregulated in the $SS^{Xdh-/-}$ rat kidney RNA seq data (*Z* score 2.887, p-values 9.24E-05) (Table S10). Moreover, NFκB signaling (*Z* score 4.636, p-value 9.24E-05), Toll-like receptor signaling (*Z* score 3.545, p-value 2.96E-04), and Stat3 signaling (*Z* score 2.795, p-value 4.87E-07) were significantly upregulated further suggesting the activation of inflammation.

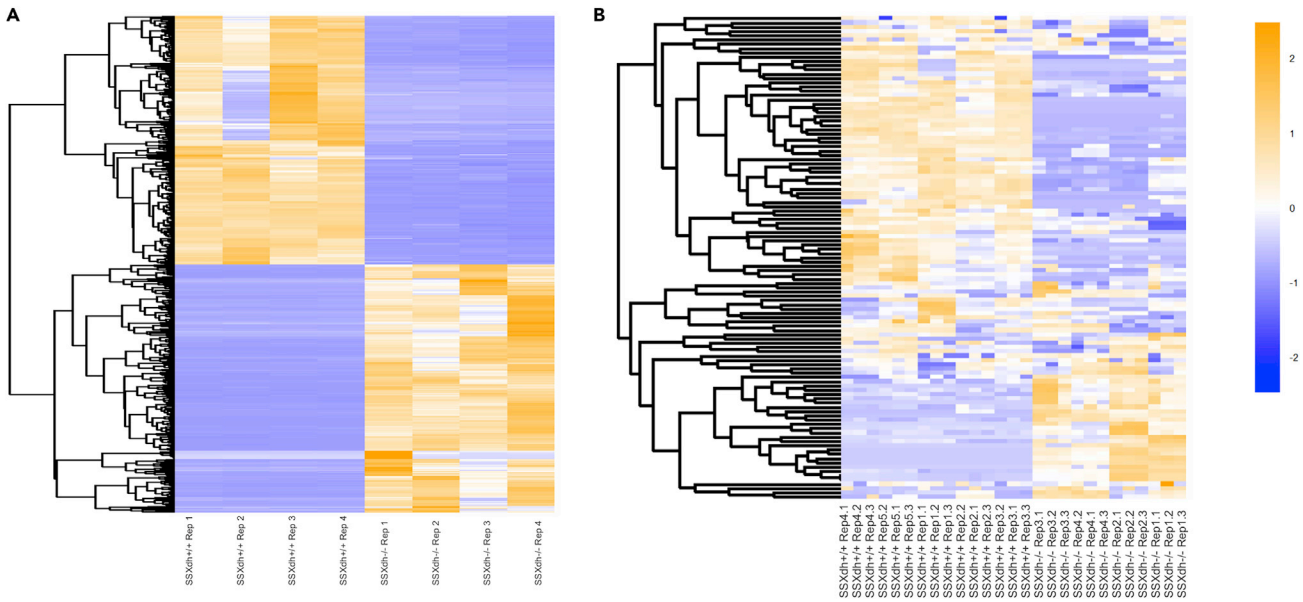

Figure 3. Data distribution of RNA sequencing and untargeted metabolomics

(A) Hierarchical clustering heatmaps of differentially expressed genes (N = 4 per group), (B) metabolites (Adjusted p < 0.05) by comparing the $SS^{Xdh-/-}$ (N = 5) and $SS^{Xdh+/+}$ (N = 4). All data are from male 6-week-old rats. Heatmap color representation: Blue- downregulation, Orange- upregulation. The color intensity represents the level of change in expression. NB: For representation, data acquired by negative HILIC ionization mode are shown for metabolomics. Data from all 4 different ionization modes have been used for further analyses.)

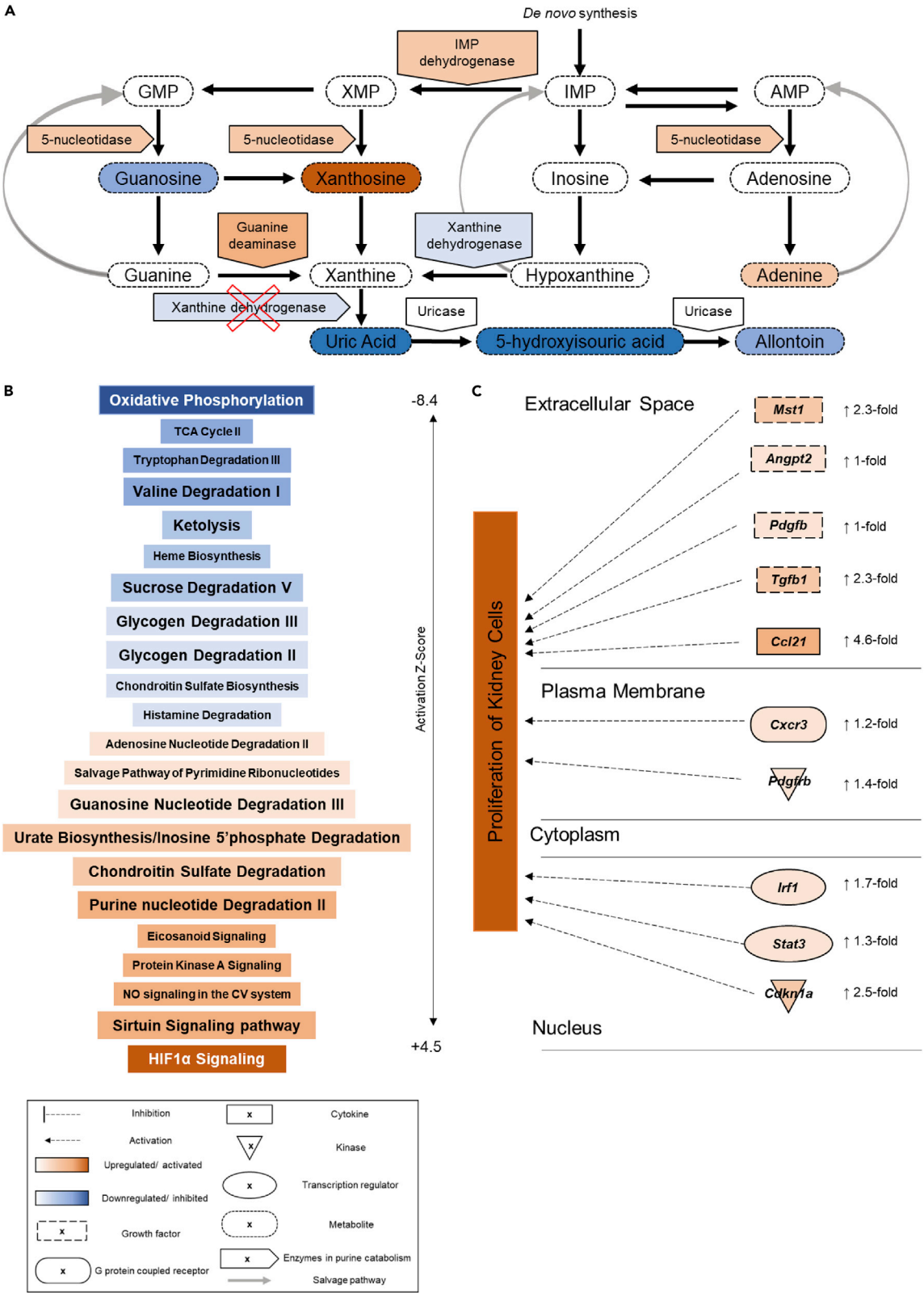
A
De novo synthesis
IMP dehydrogenase
GMP
XMP
IMP
AMP
5-nucleotidase
5-nucleotidase
5-nucleotidase
Guanosine
Xanthosine
Inosine
Adenosine
Guanine deaminase
Xanthine dehydrogenase
Guanine
Xanthine
Hypoxanthine
Adenine
Xanthine dehydrogenase
Uricase
Uricase
Uric Acid
5-hydroxyisouric acid
Allontoin
B
Oxidative Phosphorylation
TCA Cycle II
Tryptophan Degradation III
Valine Degradation I
Ketolysis
Heme Biosynthesis
Sucrose Degradation V
Glycogen Degradation III
Glycogen Degradation II
Chondroitin Sulfate Biosynthesis
Histamine Degradation
Adenosine Nucleotide Degradation II
Salvage Pathway of Pyrimidine Ribonucleotides
Guanosine Nucleotide Degradation III
Urate Biosynthesis/Inosine 5'phosphate Degradation
Chondroitin Sulfate Degradation
Purine nucleotide Degradation II
Eicosanoid Signaling
Protein Kinase A Signaling
NO signaling in the CV system
Sirtuin Signaling pathway
HIF1α Signaling
-8.4
Activation Z-Score
+4.5
Inhibition
Activation
Upregulated/ activated
Downregulated/ inhibited
Growth factor
G protein coupled receptor
Cytokine
Kinase
Transcription regulator
Metabolite
Enzymes in purine catabolism
Salvage pathway
C
Extracellular Space
Mst1
↑ 2.3-fold
Angpt2
↑ 1-fold
Pdgfb
↑ 1-fold
Tgfb1
↑ 2.3-fold
Ccl21
↑ 4.6-fold
Proliferation of Kidney Cells
Plasma Membrane
Cxcr3
↑ 1.2-fold
Pdgfrb
↑ 1.4-fold
Cytoplasm
Irf1
↑ 1.7-fold
Stat3
↑ 1.3-fold
Cdkn1a
↑ 2.5-fold
Nucleus

Figure 4. Integrated metabolomics and transcriptomics analyses of the $SS^{Xdh-/-}$ rat kidney cortex in comparison to the $SS^{Xdh+/+}$ rat

(A) Metabolite and gene fold changes in the purine catabolic pathway. Metabolites and genes that are upregulated or downregulated significantly in the $SS^{Xdh-/-}$ rat are in color-filled shapes.

(B) Top overlapping canonical pathways between the metabolomic and transcriptomic analyses. The top 22 by activation z-score are shown. For the full list see Table S1.

(C) Significantly deferentially expressed genes in $SS^{Xdh-/-}$ rats that are suggested to activate kidney cell proliferation. The color intensity represents the activation z-score for functions/pathways and fold change for genes/metabolites. For comprehensive lists of pathological functions, genes and metabolites lists see Tables S2–S10.

Lack of damage in liver and cardiac tissue in the $SS^{Xdh-/-}$ rat

Even though we saw extensive damage in the kidneys, other organs including the liver and the heart of the $SS^{Xdh-/-}$ rats appeared normal on the macroscopic level. As purine catabolism occurs in the liver, we were interested in investigating if the liver shows any signs of damage histologically. Fibrosis was not observed in $SS^{Xdh-/-}$ liver tissue stained with MT (Figure S2A). In the transcriptomics data, "liver damage" was suggested to be downregulated (*Z* score −1.32, p 8.06E-09) providing insights into this observation. We have highlighted the genes such as *Nos2*, *Il10*, and *Il1rn* that are potentially causing this protection (Figure S2B). Similarly, "heart injury" was suggested to be downregulated (*Z* score −1.45, p 7.79E-02), possibly influenced by increased expression of *Il1a*, *Serping1*, *Adora1*, *Anxa1*, *and Alox12* (Figure S3A). Heart tissue histology did not show an increase in fibrosis in the homozygous rats, corresponding with the pathway analysis (Figure S3B). The heart weights of the $SS^{Xdh-/-}$ rats were significantly smaller compared to $SS^{Xdh+/+}$ rats likely owing to their smaller body sizes (Figure S3C). "Liver damage" and "Heart injury" are terms in the IPA bio-functions list. It is worth noting that the omics data come from kidney tissue and not cardiac/liver tissue.

Downregulation of uric acid transport in the $SS^{Xdh-/-}$ rat kidneys

Urat1 encoded by *Slc22a12* and Glut9 encoded by *Slc2a9* are the main UA transporters on the apical and basolateral sides of the proximal tubule epithelium, respectively. Other basolateral UA transporters include Abcg2, Npt1, Npt4, and Oat10. The Na^+/H^+ exchanger and its regulators Nherf1 and Nherf3 have also been shown to regulate UA transport (Cunningham et al., 2007; Weinman et al., 2006). $SS^{Xdh-/-}$ rats had decreased Urat1 and Nherf1 protein levels in the renal cortex (Figure 5A). Interestingly, there was a lack of the regular Glut9 protein at 55kDa and an increased band around 70kDa in Western blots from $SS^{Xdh-/-}$ rats (Figure 5A). In the transcriptomics data, it was evident that most of the transporters (*Abcg2*, *Slc2a9*, *Slc17a3*, *Slc22a12*, *Slc9a3*) and regulatory factors (*Pdzk1*, *Slc9a3r1*) involved in UA transport are significantly downregulated in the hypouricemic rats (Figures 5B and 5C). In IPA, upstream regulators are suggested based on the overall changes seen in a particular omics analysis to provide possible mechanisms behind an observation. Interestingly, in the upstream regulators of the metabolomic profile, *Slc17a3* was predicted as the most likely candidate (Table S6).

When challenged with a high salt diet, the $SS^{Xdh-/-}$ rats fail to survive

Because changes in blood UA levels are a risk factor for hypertension and CVD in patients with CKD (Johnson et al., 2018), we examined the effect of hypouricemia on salt-sensitive hypertension by using 10-week-old male $SS^{Xdh+/+}$, $SS^{Xdh+/-}$ and $SS^{Xdh-/-}$ rats. When challenged with a high salt (HS) diet to induce hypertension, the homozygous rats failed to survive (Figure 6A). Although both wild-type and heterozygous animals developed hypertension, we did not observe a significant difference in blood pressure between the two groups over 3 weeks (Figure 6B). Based on the hypothesis that the $SS^{Xdh-/-}$ rats fail to survive on HS owing to the poor regulation of electrolyte homeostasis, we challenged an additional group of $SS^{Xdh+/+}$ and $SS^{Xdh-/-}$ rats for 3 days and collected their urine (on start and endpoint) and plasma (endpoint). Plasma Na^+ and Creatinine were significantly elevated and Ca^{2+} was significantly reduced in the $SS^{Xdh-/-}$ rats after HS consumption for 3 days (Table 3). In $SS^{Xdh-/-}$ rats, HS consumption resulted in a significant decrease in K^+ excretion and a significant increase in Na^+ and Cl^- excretion (Table 4). Comparing the $SS^{Xdh+/+}$ and $SS^{Xdh-/-}$ rats at the endpoint revealed a significant increase in Na^+ and Cl^- excretion in the homozygotes (Table 4).

DISCUSSION

Our aim in these studies was to understand the physiological and molecular mechanisms of uric acid dysregulation in CKD. By utilizing a novel rat model of *Xdh* deletion in the Dahl SS rat background, we were able to offer insights into how it can lead to kidney damage. The $SS^{Xdh-/-}$ rat is a model of hypouricemia with hypouricosuria and therefore represents conditions in which urate production is inhibited rather than

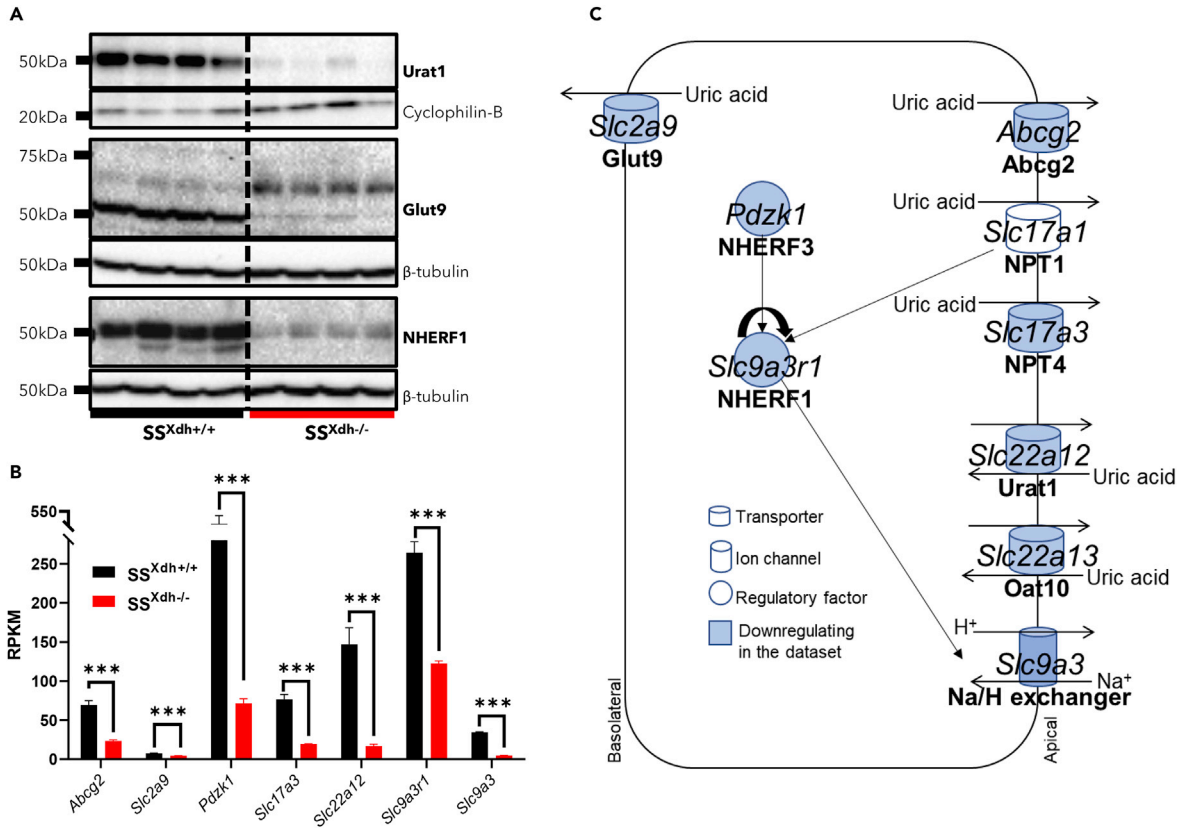

Figure 5. Changes in kidney uric acid transport in SS$^{Xdh-/-}$ rats

(A) Western blotting analysis of main transporters of UA in the kidney (Each band = one rat).

(B) Gene count of genes encoding uric acid transporters, ion channels, and regulatory factors (NS- not significant, * ≤0.05, ** ≤0.01, *** ≤0.001, **** ≤ 0.0001. Data are represented as mean ± SEM).

(C) Schematic representation of the gene expression changes in UA transport and regulation based on transcriptomic analysis. The color filled shapes represent the downregulation of genes.

excretion is increased. This is the first rat model of *Xdh* deletion and the first hypouricemic model on a SS background. There have been *Xdh* KO mouse models (XOR$^{-/-}$) created previously that failed to thrive and survive beyond 4-6 weeks (Ohtsubo et al., 2004, 2009; Vorbach et al., 2002). In one of the mouse models, investigators also reported that the pups died owing to heterozygous moms being unable to feed them, highlighting the role of XOR in lactation and attributing the lower survival to starvation (Vorbach et al., 2002). In our rat model, survival probability at the 6-week time point was ~70%, whereas theirs was nearly zero (Ohtsubo et al., 2004). Moreover, the surviving SS$^{Xdh-/-}$ rats were able to continue if they were not challenged with dietary or other interventions allowing us to conduct chronic studies. Our multi-omics pathway analyses indicated that these rats have a decreased production of energy with inhibited oxidative phosphorylation and TCA cycle, contributing to their failure to thrive. The XOR$^{-/-}$ mouse model had an increase in the urinary excretion of hypoxanthine with a decrease of xanthine before their demise (Hosoyamada et al., 2020). Because hypoxanthine inhibits the synthesis of NAD$^+$, investigators tried to rescue the XOR$^{-/-}$ mice by replenishing NAD$^+$; however, it failed owing to the lack of intestinal absorption (Hosoyamada et al., 2020). Nevertheless, the depletion of NAD$^+$ also suggests that a lack of energy production contributes to the failure to survive in hypouricemia.

We demonstrated that the lack of Xdh can lead to tubulointerstitial and glomerular damage accompanied by fibrosis in the kidney. The SS$^{Xdh-/-}$ rats lacked differentiation between the cortical and medullary areas. Rats, unlike humans, continue their kidney maturation process postnatally. On the postnatal day-21, rats normally achieve the defined areas in the kidney histologically. Lack of this differentiation at 6 weeks of age shows a disruption of kidney development in the SS$^{Xdh-/-}$ rat. Therefore, the severe renal histopathology we see could be a combination of immature kidneys and further insults leading to

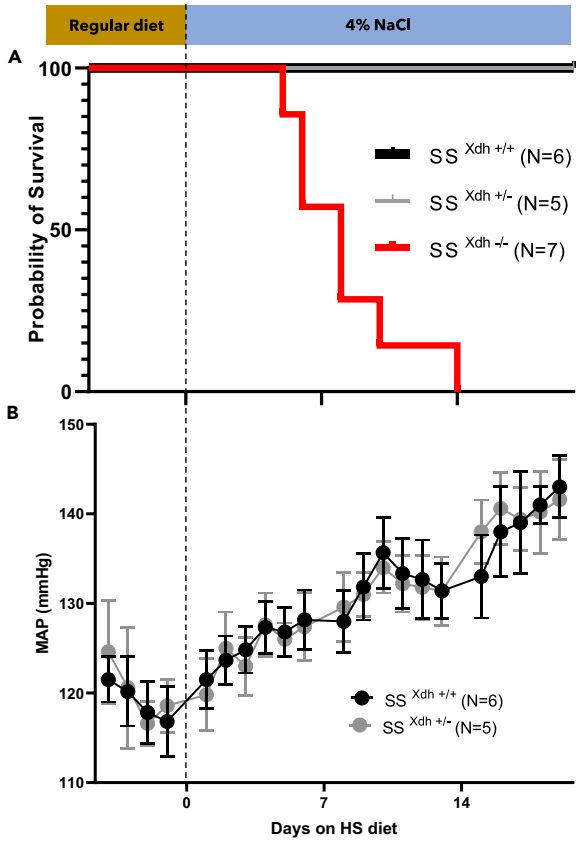

Figure 6. High salt (HS/4% NaCl) Challenge

(A) Survival probability of the $SS^{Xdh+/+}$, $SS^{Xdh+/-}$ and $SS^{Xdh-/-}$ rats (B) Mean arterial blood pressure in $SS^{Xdh+/+}$ and $SS^{Xdh+/-}$ rats on a 21-day HS diet. Data are represented as mean ± SEM.

fibrosis. Further studies at earlier time points are needed to determine the impact of developmental delays.

Primary epithelial cell culture from $XOR^{-/-}$ mice readily transformed into myofibroblasts suggesting epithelial to mesenchymal transition (EMT) activated by Tgfβ1 as the mechanism behind the fibrosis (Ohtsubo et al., 2009). Contrasting these findings, some researchers, using genetic tagging and tracking epithelial cells with electron microscopy in a transgenic mouse model overexpressing Tgfβ1, have shown evidence against EMT's involvement in fibrosis (Koesters et al., 2010). Nevertheless, in our $SS^{Xdh-/-}$ rats, we saw increased expression of *Tgfβ1*, which might be causing renal fibrosis through either EMT or other mechanisms. Additionally, we found that *Ccl21* and *Stat3* were significantly upregulated in the $SS^{Xdh-/-}$ rat kidney. Ccl21 causes renal cell proliferation (Banas, 2002) and facilitates fibrocyte infiltration into the kidney, and contributes to ongoing fibrosis (Sakai et al., 2006). Stat3 has also been shown to activate interstitial fibrosis via profibrotic factors (Bienaimé et al., 2016). Pharmacological blockade of Stat3 improved renal function and attenuated kidney fibrosis in hyperuricemic mice (Pan et al., 2021). Interestingly, Stat3 has

Table 3. Changes in plasma electrolytes and creatinine on the 3-day HS challenge

Plasma electrolytes & Creatinine	$SS^{Xdh+/+}$ (N = 5)	$SS^{Xdh-/-}$ (N = 5)
K^+	3.62 ± 0.12 mM	3.48 ± 0.12 mM
Na^+	141 ± 0.83 mM	156 ± 2.15 mM ***
Ca^{2+}	1.32 ± 0.03 mM	0.86 ± 0.07 mM ***
Cl^-	121 ± 18 mM	126 ± 6 mM
Creatinine	0.36 ± 0.01 mg/dL	1.51 ± 0.14 mg/dL **

Table 4. Changes in electrolyte and creatinine excretion on the 3-day HS challenge

Amount excreted in 24 h (mmol/24h)	LS/SS$^{Xdh+/+}$ (N = 5) *	LS/SS$^{Xdh-/-}$ (N = 5)$^{\#}$	HS/SS$^{Xdh+/+}$ (N = 5) ^	HS/SS$^{Xdh-/-}$ (N = 5)
K^+	3.08 ± 0.12	1.83 ± 0.12 *	0.81 ± 0.14 ***	0.69 ± 0.04$^{\#\#\#}$
Na^+	0.31 ± 0.04	0.23 ± 0.01	9.19 ± 0.80 ***	5.43 ± 0.49$^{\#\wedge}$
Ca^{2+}	0.002 ± 0.00	0.02 ± 0.00 **	0.04 ± 0.00 *	0.05 ± 0.01
Cl^-	5.70 ± 0.70	0.86 ± 0.01*	8.94 ± 0.76 *	5.13 ± 0.43 ^^^
Creatinine	3.09 ± 0.12	0.02 ± 0.00 ***	0.05 ± 0.01 *	0.02 ± 0.00

LS, on a low salt diet; HS, on a high salt diet. p-value: * Comparison with LS/SS$^{Xdh+/+}$. $^{\#}$ Comparison with LS/SS$^{Xdh-/-}$. ^ Comparison with LS/SS$^{Xdh+/+}$. Underlined means include values below the sensitivity of the test. Data are represented as mean ± SEM.

shown a protective effect on liver injury (Klein et al., 2005). Therefore, Stat3 might be responsible for the presence of kidney damage and lack of liver damage in our model. Stat3 expression in the liver itself should be investigated further to draw direct conclusions.

Our metabolomics data, both in kidney and urine, showed that the lack of Xdh can cause the accumulation of upstream purine and other intermediate metabolites. The crystals observed in the homozygous rat kidneys are likely made up of these metabolites. These crystals potentially caused damage to the tubules resulting in the infiltration of immune cells and inflammation. Pro-fibrotic and pro-proliferative growth factors, cytokines, and chemokines are produced consequentially in an inflammatory response which aligns with our findings (Mattson, 2014).

We hypothesized that lack of UA will increase ROS, contributing to kidney damage. UA is known to be a potent antioxidant in circulation (Ames et al., 1981) by being a scavenger of carbon-centered radicals and peroxyl radicals (eg. peroxynitrite). UA is also known to protect erythrocyte membranes against lipid peroxidation (Chen et al., 2016). The multi-omics pathway analyses suggested an increase in oxidative stress. As plasma and kidney tissue levels of UA were lacking in the model, ROS accumulation is another factor potentially contributing to the damage. Furthermore, *Cat*, the gene encoding for catalase was significantly downregulated in our RNA seq data, suggesting that H_2O_2 might be accumulating in the kidneys. Previous studies conducted using Dahl SS rat have shown that Nox4 is a contributor to kidney injury and knocking out *Nox4* decreases H_2O_2 and oxidative stress caused by it (Cowley et al., 2016; Ilatovskaya et al., 2018). Further studies are necessary to make conclusions about the particular type of ROS that is adding to kidney damage in our model.

Moreover, SS$^{Xdh-/-}$ rats demonstrated smaller isolated areas of preserved tubules surrounded by interstitial fibrosis. The build-up of fibrotic tissue can mechanically protect the nephrons from getting damaged further in the initial stages of damage as the accumulation of collagen happens as a supportive mechanism in wound healing (Wynn, 2008). Eventually, compensatory mechanisms fail to preserve the nephron structure, and kidney function declines. Accordingly, we saw that hypouricemic rats failed to manage electrolyte homeostasis. The increased plasma creatinine indicated the declining GFR and overall renal function.

RNA seq data and protein levels suggest that the expression of UA transporters was downregulated in the hypouricemic rat. Nherf1 has been shown to interact with Urat1 to regulate UA transport (Cunningham et al., 2007), and lack of the protein has been shown to cause UA and phosphate wasting (Weinman et al., 2006). We demonstrated that SS$^{Xdh-/-}$ rats have a decrease in Nherf1 which regulates the Na/H exchanger. Interestingly, Glut9, the basolateral UA transporter, showed downregulation in RNA and post-translational modification of the protein. Glut9 is a highly glycosylated protein (Mandal and Mount, 2019; Pyla et al., 2013), and we believe SS$^{Xdh-/-}$ rats are showing a compensatory change in the form of glycosylation. Several other ion channel encoding genes were significantly changing in the transcriptomics profile. These changes are likely affecting the electrolyte and water balance contributing to the dramatic functional decline we are seeing.

Renal XOR activity has been shown to concomitantly increase with the increase in salt intake in the Dahl SS rats (Laakso et al., 1998). Furthermore, salt-resistant Sprague-Dawley rats exposed to higher levels of UA

have been shown to later develop salt sensitivity (Watanabe et al., 2002). These studies draw attention to a connection between SS hypertension and UA, but whether it is a result or a causal factor is unclear. In our studies, we attempted to examine the development of SS hypertension in the context of hypouricemia. The level of kidney damage and functional decline in the $SS^{Xdh-/-}$ rats prevented them from surviving an HS challenge.

In summary, we established a novel rat model of hypouricemia with a KO in the *Xdh* gene. This animal model demonstrated better survival than previous models with the deletion of Xdh, allowing for more in-depth chronic studies. We conclude that the genetic ablation of the Xdh gene leads to kidney damage and functional decline through the accumulation of purine metabolites and oxidative stress. These data strengthen the idea that UA is not merely a harmful waste product but also a beneficial antioxidant and should be regulated well for better CKD outcomes. Moreover, it highlights the importance of UA homeostasis in maintaining renal function and energy production. Using the genes, metabolites, and pathways emphasized by the multi-omics analyses, future studies into the mechanism of UA deregulation are necessary.

Limitations of the study

The limitation of these studies in translating to human health comes from the differences between purine metabolism in humans and rodents. Humans have a mutation in the *UO* gene encoding the uricase enzyme. Uricase catalyzes the oxidation of UA into 5-hydroxyisourate and allantoin. Lack of uricase makes humans naturally and mildly hyperuricemic; therefore, hypouricemia is a rare condition for humans. The fractional excretion of uric acid differs greatly between humans (~10%) and rats (~40%) as well (Roch-Ramel et al., 1976). Nevertheless, in epidemiological studies, it is shown that both hyper- and hypouricemia are associated with higher mortality in CKD (Suliman et al., 2006) and a higher risk of kidney function decline in healthy people (Kanda et al., 2015). However, hypouricemia has not been studied nearly enough to understand how it can lead to kidney damage. Furthermore, UA lowering therapy is being considered for patients with CKD without gout (Sato et al., 2019) which warrants a deeper understanding of the consequences of decreased UA levels.

STAR★METHODS

Detailed methods are provided in the online version of this paper and include the following:

- KEY RESOURCES TABLE
- RESOURCE AVAILABILITY
  - Lead contact
  - Materials availability
  - Data and code availability
- EXPERIMENTAL MODEL AND SUBJECT DETAILS
  - Animals
- METHOD DETAILS
  - Western blotting
  - Histology, immunohistochemistry
  - Assessment of pathology
  - RNA sequencing
  - Untargeted metabolomics
  - Omics data visualization and pathway analysis
- QUANTIFICATION AND STATISTICAL ANALYSIS

SUPPLEMENTAL INFORMATION

Supplemental information can be found online at https://doi.org/10.1016/j.isci.2022.104887.

ACKNOWLEDGMENTS

We gratefully acknowledge Dr. Elena Isaeva, Dr. Sherif Khedr, and Tessa Shankey for technical assistance with experiments; Oksana Nikolaienko for the glomerular scoring analysis; MCW Mellowes Genomic Sciences and Precision Medicine Center for performing RNA seq; Children's Research Institute Histology Core at the MCW for processing tissue for immunohistochemistry, and the Mayo Clinic metabolomics

core for performing untargeted metabolomic analysis. This research was supported by the National Institutes of Health grants R35 HL135749 (to AS), R01 DK126720 (to OP), R24 HL114474 (to MD), Department of Veterans Affairs grant I01 BX004024 (to AS), and endowed funds from the SC SmartState Centers of Excellence (to OP).

AUTHOR CONTRIBUTIONS

LVD, AS, OP, and AE-M conceptualized the study. LVD, AS, and OP designed the study; AMG and MRD created the animal model; LVD, AZ, VL, and DRS carried out experiments; LVD and OP analyzed the data; MB visualized data; LVD prepared the figures; LVD, AS, and OP drafted and revised the article. All authors approved the final version of the article.

DECLARATION OF INTERESTS

The authors declare no competing interests.

Received: June 15, 2022
Revised: June 20, 2022
Accepted: August 2, 2022
Published: September 16, 2022

REFERENCES

Ames, B.N., Cathcart, R., Schwiers, E., and Hochstein, P. (1981). Uric acid provides an antioxidant defense in humans against oxidant- and radical-caused aging and cancer: a hypothesis. Proc. Natl. Acad. Sci. USA *78*, 6858–6862.

Banas, Bernhard, et al. (2002). Roles of SLC/CCL21 and CCR7 in Human Kidney for Mesangial Proliferation, Migration, Apoptosis, and Tissue Homeostasis. The Journal of Immunology. https://doi.org/10.4049/jimmunol.168.9.4301.

Bienaimé, F., Muorah, M., Yammine, L., Burtin, M., Nguyen, C., Baron, W., Garbay, S., Viau, A., Broueilh, M., Blanc, T., et al. (2016). Stat3 controls tubulointerstitial communication during CKD. J. Am. Soc. Nephrol. *27*, 3690–3705. https://doi.org/10.1681/asn.2015091014.

Cappola, T.P., Kass, D.A., Nelson, G.S., Berger, R.D., Rosas, G.O., Kobeissi, Z.A., Marbán, E., and Hare, J.M. (2001). Allopurinol improves myocardial efficiency in patients with idiopathic dilated cardiomyopathy. Circulation *104*, 2407–2411. https://doi.org/10.1161/hc4501.098928.

Chen, C., Lu, J.M., and Yao, Q. (2016). Hyperuricemia-related diseases and xanthine oxidoreductase (XOR) inhibitors: an overview. Med. Sci. Monit. *22*, 2501–2512.

Cowley, A.W., Jr., Yang, C., Zheleznova, N.N., Staruschenko, A., Kurth, T., Rein, L., Kumar, V., Sadovnikov, K., Dayton, A., Hoffman, M., et al. (2016). Evidence of the importance of Nox4 in production of hypertension in Dahl salt-sensitive rats. Hypertension *67*, 440–450. https://doi.org/10.1161/hypertensionaha.115.06280.

Cunningham, R., Brazie, M., Kanumuru, S., E, X., Biswas, R., Wang, F., Steplock, D., Wade, J.B., Anzai, N., Endou, H., et al. (2007). Sodium-hydrogen exchanger regulatory factor-1 interacts with mouse urate transporter 1 to regulate renal proximal tubule uric acid transport. J. Am. Soc. Nephrol. *18*, 1419–1425. https://doi.org/10.1681/asn.2006090980.

Feig, D.I., Soletsky, B., and Johnson, R.J. (2008). Effect of allopurinol on blood pressure of adolescents with newly diagnosed essential hypertension: a randomized trial. JAMA *300*, 924–932. https://doi.org/10.1001/jama.300.8.924.

Fujinaga, S., Ito, A., Nakagawa, M., Watanabe, T., Ohtomo, Y., and Shimizu, T. (2013). Posterior reversible encephalopathy syndrome with exercise-induced acute kidney injury in renal hypouricemia type 1. Eur. J. Pediatr. *172*, 1557–1560. https://doi.org/10.1007/s00431-013-1986-7.

Gardiner, L., Akintola, A., Chen, G., Catania, J.M., Vaidya, V., Burghardt, R.C., Bonventre, J.V., Trzeciakowski, J., and Parrish, A.R. (2012). Structural equation modeling highlights the potential of Kim-1 as a biomarker for chronic kidney disease. Am. J. Nephrol. *35*, 152–163. https://doi.org/10.1159/000335579.

Gewin, L., Zent, R., and Pozzi, A. (2017). Progression of chronic kidney disease: too much cellular talk causes damage. Kidney Int. *91*, 552–560. https://doi.org/10.1016/j.kint.2016.08.025.

Harijith, A., Ebenezer, D.L., and Natarajan, V. (2014). Reactive oxygen species at the crossroads of inflammasome and inflammation. Front. Physiol. *5*, 352. https://doi.org/10.3389/fphys.2014.00352.

Hosoya, T., Uchida, S., Shibata, S., Tomioka, N.H., Matsumoto, K., and Hosoyamada, M. (2022). Xanthine oxidoreductase inhibitors suppress the onset of exercise-induced AKI in high HPRT activity *Urat1*- double knockout mice. J. Am. Soc. Nephrol. *33*, 326–341. https://doi.org/10.1681/asn.2021050616.

Hosoyamada, M., Tomioka, N.H., Ohtsubo, T., and Ichida, K. (2020). Xanthine oxidoreductase knockout mice with high HPRT activity were not rescued by NAD(+) replenishment. Nucleosides Nucleotides Nucleic Acids *39*, 1465–1473. https://doi.org/10.1080/15257770.2020.1725044.

Ichida, K., Hosoyamada, M., Hisatome, I., Enomoto, A., Hikita, M., Endou, H., and Hosoya, T. (2004). Clinical and molecular analysis of patients with renal hypouricemia in Japan-influence of URAT1 gene on urinary urate excretion. J. Am. Soc. Nephrol. *15*, 164–173. https://doi.org/10.1097/01.asn.0000105320.04395.d0.

Ilatovskaya, D.V., Blass, G., Palygin, O., Levchenko, V., Pavlov, T.S., Grzybowski, M.N., Winsor, K., Shuyskiy, L.S., Geurts, A.M., Cowley, A.W., Jr., et al. (2018). A NOX4/TRPC6 pathway in podocyte calcium regulation and renal damage in diabetic kidney disease. J. Am. Soc. Nephrol. *29*, 1917–1927. https://doi.org/10.1681/asn.2018030280.

Ishikawa, I., Sakurai, Y., Masuzaki, S., Sugishita, N., Shinoda, A., and Shikura, N. (1990). Exercise-induced acute renal failure in 3 patients with renal hypouricemia. Nihon Jinzo Gakkai Shi *32*, 923–928.

Izzedine, H., Launay-Vacher, V., Isnard-Bagnis, C., and Deray, G. (2003). Drug-induced Fanconi's syndrome. Am. J. Kidney Dis. *41*, 292–309. https://doi.org/10.1053/ajkd.2003.50037.

Johnson, R.J., Bakris, G.L., Borghi, C., Chonchol, M.B., Feldman, D., Lanaspa, M.A., Merriman, T.R., Moe, O.W., Mount, D.B., Sanchez Lozada, L.G., et al. (2018). Hyperuricemia, acute and chronic kidney disease, hypertension, and cardiovascular disease: report of a scientific workshop organized by the national kidney foundation. Am. J. Kidney Dis. *71*, 851–865. https://doi.org/10.1053/j.ajkd.2017.12.009.

Kalari, K.R., Nair, A.A., Bhavsar, J.D., O'Brien, D.R., Davila, J.I., Bockol, M.A., Nie, J., Tang, X., Baheti, S., Doughty, J.B., et al. (2014). MAP-RSeq: Mayo analysis pipeline for RNA sequencing. BMC Bioinf. *15*, 224. https://doi.org/10.1186/1471-2105-15-224.

Kanda, E., Muneyuki, T., Kanno, Y., Suwa, K., and Nakajima, K. (2015). Uric acid level has a U-shaped association with loss of kidney function in healthy people: a prospective cohort study.

PLoS One *10*, e0118031. https://doi.org/10.1371/journal.pone.0118031.

Klein, C., Wüstefeld, T., Assmus, U., Roskams, T., Rose-John, S., Müller, M., Manns, M.P., Ernst, M., and Trautwein, C. (2005). The IL-6-gp130-STAT3 pathway in hepatocytes triggers liver protection in T cell-mediated liver injury. J. Clin. Invest. *115*, 860–869. https://doi.org/10.1172/jci23640.

Koesters, R., Kaissling, B., LeHir, M., Picard, N., Theilig, F., Gebhardt, R., Glick, A.B., Hähnel, B., Hosser, H., Gröne, H.J., and Kriz, W. (2010). Tubular overexpression of transforming growth factor-β1 induces autophagy and fibrosis but not mesenchymal transition of renal epithelial cells. Am. J. Pathol. *177*, 632–643. https://doi.org/10.2353/ajpath.2010.091012.

Kuwabara, M., Niwa, K., Ohtahara, A., Hamada, T., Miyazaki, S., Mizuta, E., Ogino, K., and Hisatome, I. (2017). Prevalence and complications of hypouricemia in a general population: a large-scale cross-sectional study in Japan. PLoS One *12*, e0176055. https://doi.org/10.1371/journal.pone.0176055.

Laakso, J., Mervaala, E., Himberg, J.J., Teräväinen, T.L., Karppanen, H., Vapaatalo, H., and Lapatto, R. (1998). Increased kidney xanthine oxidoreductase activity in salt-induced experimental hypertension. Hypertension *32*, 902–906.

Lee, S.Y., Park, W., Suh, Y.J., Lim, M.J., Kwon, S.-R., Lee, J.-H., Joo, Y.B., Oh, Y.-K., and Jung, K.-H. (2019). Association of serum uric acid with cardiovascular disease risk scores in Koreans. Int. J. Environ. Res. Public Health *16*, 4632. https://doi.org/10.3390/ijerph16234632.

Mandal, A.K., and Mount, D.B. (2019). Interaction between ITM2B and GLUT9 links urate transport to neurodegenerative disorders. Front. Physiol. *10*, 1323. https://doi.org/10.3389/fphys.2019.01323.

Mattson, D.L. (2014). Infiltrating immune cells in the kidney in salt-sensitive hypertension and renal injury. Am. J. Physiol. Renal Physiol. *307*, F499–F508. https://doi.org/10.1152/ajprenal.00258.2014.

Michelis, M.F., Warms, P.C., Fusco, R.D., and Davis, B.B. (1974). Hypouricemia and hyperuricosuria in Laennec cirrhosis. Arch. Intern. Med. *134*, 681–683.

Mishra, S.R., Mahapatra, K.K., Behera, B.P., Patra, S., Bhol, C.S., Panigrahi, D.P., Praharaj, P.P., Singh, A., Patil, S., Dhiman, R., and Bhutia, S.K. (2021). Mitochondrial dysfunction as a driver of NLRP3 inflammasome activation and its modulation through mitophagy for potential therapeutics. Int. J. Biochem. Cell Biol. *136*, 106013. https://doi.org/10.1016/j.biocel.2021.106013.

Ohta, T., Sakano, T., Igarashi, T., Itami, N., and Ogawa, T.; ARF Assocoated with Renal Hypouricemia Research Group (2004). Exercise-induced acute renal failure associated with renal hypouricaemia: results of a questionnaire-based survey in Japan. Nephrol. Dial. Transplant. *19*, 1447–1453. https://doi.org/10.1093/ndt/gfh094.

Ohtsubo, T., Matsumura, K., Sakagami, K., Fujii, K., Tsuruya, K., Noguchi, H., Rovira, I.I., Finkel, T., and Iida, M. (2009). Xanthine oxidoreductase depletion induces renal interstitial fibrosis through aberrant lipid and purine accumulation in renal tubules. Hypertension *54*, 868–876. https://doi.org/10.1161/hypertensionaha.109.135152.

Ohtsubo, T., Rovira, I.I., Starost, M.F., Liu, C., and Finkel, T. (2004). Xanthine oxidoreductase is an endogenous regulator of cyclooxygenase-2. Circ. Res. *95*, 1118–1124. https://doi.org/10.1161/01.RES.0000149571.96304.36.

Pan, J., Shi, M., Guo, F., Ma, L., and Fu, P. (2021). Pharmacologic inhibiting STAT3 delays the progression of kidney fibrosis in hyperuricemia-induced chronic kidney disease. Life Sci. *285*, 119946. https://doi.org/10.1016/j.lfs.2021.119946.

Pineda, C., Soto-Fajardo, C., Mendoza, J., Gutiérrez, J., and Sandoval, H. (2019). Hypouricemia: what the practicing rheumatologist should know about this condition. Clin. Rheumatol. *39*, 135–147. https://doi.org/10.1007/s10067-019-04788-8.

Priante, G., Gianesello, L., Ceol, M., Del Prete, D., and Anglani, F. (2019). Cell death in the kidney. Int. J. Mol. Sci. *20*, 3598.

Pyla, R., Poulose, N., Jun, J.Y., and Segar, L. (2013). Expression of conventional and novel glucose transporters, GLUT1, -9, -10, and -12, in vascular smooth muscle cells. Am. J. Physiol. Cell Physiol. *304*, C574–C589. https://doi.org/10.1152/ajpcell.00275.2012.

Robinson, M.D., McCarthy, D.J., and Smyth, G.K. (2009). edgeR: a Bioconductor package for differential expression analysis of digital gene expression data. Bioinformatics *26*, 139–140. https://doi.org/10.1093/bioinformatics/btp616.

Roch-Ramel, F., Diezi-Chomety, F., De Rougemont, D., Tellier, M., Widmer, J., and Peters, G. (1976). Renal excretion of uric acid in the rat: a micropuncture and microperfusion study. Am. J. Physiol. *230*, 768–776. https://doi.org/10.1152/ajplegacy.1976.230.3.768.

Sakai, N., Wada, T., Yokoyama, H., Lipp, M., Ueha, S., Matsushima, K., and Kaneko, S. (2006). Secondary lymphoid tissue chemokine (SLC/CCL21)/CCR7 signaling regulates fibrocytes in renal fibrosis. Proc. Natl. Acad. Sci. U. S. A. *103*, 14098–14103. https://doi.org/10.1073/pnas.0511200103.

Sato, Y., Feig, D.I., Stack, A.G., Kang, D.-H., Lanaspa, M.A., Ejaz, A.A., Sánchez-Lozada, L.G., Kuwabara, M., Borghi, C., and Johnson, R.J. (2019). The case for uric acid-lowering treatment in patients with hyperuricaemia and CKD. Nat. Rev. Nephrol. *15*, 767–775. https://doi.org/10.1038/s41581-019-0174-z.

Shirakura, T., Nomura, J., Matsui, C., Kobayashi, T., Tamura, M., and Masuzaki, H. (2016). Febuxostat, a novel xanthine oxidoreductase inhibitor, improves hypertension and endothelial dysfunction in spontaneously hypertensive rats. Naunyn-Schmiedeberg's Arch. Pharmacol. *389*, 831–838. https://doi.org/10.1007/s00210-016-1239-1.

Son, C.-N., Kim, J.-M., Kim, S.-H., Cho, S.-K., Choi, C.-B., Sung, Y.-K., Kim, T.-H., Bae, S.-C., Yoo, D.-H., and Jun, J.-B. (2016). Prevalence and possible causes of hypouricemia at a tertiary care hospital. Korean J. Intern. Med. *31*, 971–976. https://doi.org/10.3904/kjim.2015.125.

Suliman, M.E., Johnson, R.J., García-López, E., Qureshi, A.R., Molinaei, H., Carrero, J.J., Heimbürger, O., Bárány, P., Axelsson, J., Lindholm, B., and Stenvinkel, P. (2006). J-shaped mortality relationship for uric acid in CKD. Am. J. Kidney Dis. *48*, 761–771. https://doi.org/10.1053/j.ajkd.2006.08.019.

Trushina, E., Dutta, T., Persson, X.M.T., Mielke, M.M., and Petersen, R.C. (2013). Identification of altered metabolic pathways in plasma and CSF in mild cognitive impairment and Alzheimer's disease using metabolomics. PLoS One *8*, e63644. https://doi.org/10.1371/journal.pone.0063644.

Verdecchia, P., Schillaci, G., Reboldi, G., Santeusanio, F., Porcellati, C., and Brunetti, P. (2000). Relation between serum uric acid and risk of cardiovascular disease in essential hypertension the PIUMA study. Hypertension *36*, 1072–1078.

Vorbach, C., Scriven, A., and Capecchi, M.R. (2002). The housekeeping gene xanthine oxidoreductase is necessary for milk fat droplet enveloping and secretion: gene sharing in the lactating mammary gland. Genes Dev. *16*, 3223–3235. https://doi.org/10.1101/gad.1032702.

Watanabe, S., Kang, D.H., Feng, L., Nakagawa, T., Kanellis, J., Lan, H., Mazzali, M., and Johnson, R.J. (2002). Uric acid, hominoid evolution, and the pathogenesis of salt-sensitivity. Hypertension *40*, 355–360.

Weinman, E.J., Mohanlal, V., Stoycheff, N., Wang, F., Steplock, D., Shenolikar, S., and Cunningham, R. (2006). Longitudinal study of urinary excretion of phosphate, calcium, and uric acid in mutant NHERF-1 null mice. Am. J. Physiol. Renal Physiol. *290*, F838–F843. https://doi.org/10.1152/ajprenal.00374.2005.

Wynn, T.A. (2008). Cellular and molecular mechanisms of fibrosis. J. Pathol. *214*, 199–210. https://doi.org/10.1002/path.2277.

Xyda, S.E., Vuckovic, I., Petterson, X.M., Dasari, S., Lalia, A.Z., Parvizi, M., Macura, S.I., and Lanza, I.R. (2020). Distinct influence of omega-3 fatty acids on the plasma metabolome of healthy older adults. J. Gerontol. A Biol. Sci. Med. Sci. *75*, 875–884. https://doi.org/10.1093/gerona/glz141.

STAR★METHODS

KEY RESOURCES TABLE

REAGENT or RESOURCE	SOURCE	IDENTIFIER
Antibodies		
Xdh	ABclonal	Cat#. A13052; RRID:AB_2759900
Slc22a12	ABclonal	Cat#. A5118; RRID:AB_2766026
Slc2a9	ABclonal	Cat#. A14606; RRID:AB_2761482
Nherf1	ABclonal	Cat#. A0146; RRID:AB_2756978
Kim1	Santa Cruz Biotech	Cat#. sc-518008
HRP-conjugated β-Tubulin	ABclonal	Cat#. AC030; RRID:AB_2769870
Cyclophilin B	Cell Signaling Technology	Cat#. 43603; RRID:AB_2799247
Chemicals, peptides, and recombinant proteins		
RPMI1640	Invitrogen	Cat# 11835-030
BSA	Sigma	Cat# A3059
TRIzol	ThermoFisher	Cat# 15596026
Critical commercial assays		
Albumin Assay	Active Motif	Cat# 15002
Experimental models: Organisms/strains		
Rat: SS-Xdh^{em1Mcwi}	MCW	Rat Genome Database ID:14398479
Software and algorithms		
Fiji (ImageJ 1.47v)	National Institutes of Health, USA	https://imagej.nih.gov/ij/
SigmaPlot 12.5	Systat Software, Inc	https://systatsoftware.com/
GraphPad Prism 9.0	Dotmatics	https://www.graphpad.com/
Other		
Teklad Low Salt Mouse/Rat sterilizable Diet	Envigo	No. 7034
Custom diet (4% NaCl/ HS diet)	Dyets	No. D113756
mesh sieve 73.7 µm	Sigma	Cat# S4145
mesh sieve 150 µm	Fisher Sci	Cat# 04-881-5Z
mesh sieve 106 µm	Fisher Sci	Cat# 04-881-5X

RESOURCE AVAILABILITY

Lead contact

Further information and requests for resources and reagents should be directed to and will be fulfilled by the lead contact, Alexander Staruschenko (staruschenko@usf.edu).

Materials availability

This study did not generate new unique reagents.

Data and code availability

The datasets are available in the following databases: RNA-Seq data: Gene Expression Omnibus: GSE198642. https://www.ncbi.nlm.nih.gov/geo/query/acc.cgi?acc=GSE198642.

Any additional information required to reanalyze the data reported in this paper is available from the lead contact upon request.

EXPERIMENTAL MODEL AND SUBJECT DETAILS

Animals

All animal experiments adhered to the National Institute of Health Guide for the Care and Use of Laboratory Animals and all protocols were reviewed and approved by the Medical College of Wisconsin (MCW) IACUC. The $SS^{Xdh-/-}$ rat (SS-$Xdh^{em1Mcwi}$, Rat Genome Database ID:14398479) was created using CRISPR/Cas9 targeting the *Xdh* exon 4 genomic sequence GTTTCCTATGCCTTCCACGG in the Dahl salt-sensitive (SS/JrHsdMcwi) rat strain background. A seven-base pair frame-shift deletion in exon 4 was identified (CAGCTTCTGGGTGTTTCCTATGCCTTCC————TCACAGC) and a breeding colony was established by backcrossing to the parental strain. This mutation results in a predicted truncation of the resulting protein consisting of 88 amino acids.

Both male and female rats in all genotypes (wild-type, heterozygous and homozygous) were used for the initial characterization of the model. Specifications of which sex and genotypes were used for each of the results shown can be found in the figure legends. Rats were weaned at 3 weeks of age and kept on the Teklad Low Salt Mouse/Rat sterilizable Diet (regular diet) (Envigo, 7034). This time point was chosen based on the development of the rat kidney, weaning, and experience from previous studies. The animal tissue collections were done at 6 weeks unless otherwise specified. At 6–7 weeks of age, the rats were anesthetized, and kidneys were perfused with PBS via abdominal descending aorta canulation and ligation of celiac, mesenteric and ascending aorta. PBS was pumped in at a rate of 4 ml/min in the case of knock out animals and 6 ml/min for control animals. Washthru was released with an incision into the vena cava. After kindeys were blanched, animals were euthanized by thoracotomy tissue collected and frozen in liquid nitrogen or placed in 10% formalin for subsequent experiments.

For the high salt challenge diet was switched to 4% NaCl (HS diet) (Dyets, Inc.; D113756). The first HS challenge with blood pressure measurements was conducted for 3 weeks. The second HS challenge for electrolyte analysis was 3 days long. The 3-day period was chosen because, during the longer HS challenge, homozygous rats started dying from the 5th day. Rats that were used for chronic blood pressure measurements at 10 weeks of age were implanted with a radio telemeter (PA-C40; DSI) under anesthesia (2%–3 % (vol/vol) isoflurane). The catheter tip was placed in the abdominal aorta via the femoral artery while the transmitter was placed subcutaneously. Rats were placed on receiver pads and allowed to recover 5–6 days before the blood pressure measurement collection started via DSI system software.

At necessary time points, animals were placed in metabolic cages for 24 h urine collections. Blood was collected at the endpoint procedure. Urine and blood electrolytes (K^+, Na^+, Cl^-, Ca^{2+}) and creatinine were measured using a radiometer (ABL800 FLEX, Radiometer America Inc.). Albumin was measured by a fluorescent assay (Active Motif, Carlsbad, CA) and read by a fluorescent plate reader (FL600, Bio-Tek, Winooski, VT). Uric acid measurements were done through Idexx Bioanalytics (North Grafton, MA). The 24 h excretion of any electrolyte or protein is calculated using the concentration of the substance and the diuresis.

METHOD DETAILS

Western blotting

Snap-frozen kidney cortex pieces collected at the end-point surgery were used to prepare lysates by dissolving in Laemmli buffer with a protease inhibitor at 20 mg/ml with pulse sonication for 15–20 s. This allowed tissue to fully dissolve in the buffer without any losses in the undissolved fraction. Samples were subjected to tris-Cl SDS-PAGE, transferr onto nitrocellulose membrane (Millipore), antibody hybridized, and visualized by enhanced chemiluminescence (ECL; Amersham Biosciences). See the Key resources table for antibody details.

Histology, immunohistochemistry

Formalin-fixed kidneys, liver, and heart from the end-point surgeries were paraffin-embedded, sectioned, and mounted. Masson's Trichrome staining was used with kidney, liver, and heart tissue to visualize damage and fibrosis. Immunostaining was done using commercially available antibodies (See Key resources table). For crystal visualization, frozen kidneys were embedded in optimal cutting temperature compound and sectioned. The slides were kept in 4°C. Carl Zeiss metallurgical microscope equipped with an LED light source was used to image the crystals. The samples were examined under cross-polarized light.

Assessment of pathology

Fibrosis was quantified using color thresholding through Metamorph software (Molecular Devices, Sunnyvale, CA). Glomeruli were isolated by sequential sieving of the minced freshly isolated kidney cortex (mixed with the culture medium solution RPMI1640 (Invitrogen) with 5% BSA (RPMI-BSA solution)) through 150 μm, 106 μm (#04-881-5Z and #04-881-5X; Fisher Sci), and 73.7μm mesh sieves (#S4145; Sigma). The glomeruli left on the top of the last sieve were rinsed using the RPMI-BSA solution into a 15 ml conical tube and gravity pelleted for 10–15 min on ice. After sedimentation, the excess RPMI-BSA solution was removed, and the isolated decapsulated glomeruli were used for microscopy. Using Nikon eclipse TE2000-S microscope images of glomeruli were taken. The area of glomeruli was calculated using the Fiji image application (ImageJ 1.51u, NIH). Glomerular damage was assessed by an independent observer blinded to the study using quantitative morphometric analysis based on a scale of 0–4 as follows. On the scale, 0 represents a normal healthy kidney, 1 being 1–25% of mesangial expansion and sclerosis (mesangial expansion, thickening of the basement membrane, and/or irregular lumina of capillaries), 2 for 26–50% (mild segmental hyalinosis involving 50% of the glomerular tuft), 3 being for 51–75% (diffuse sclerosis involving 50% of the glomerular capillaries), and a score of 4 is given for 76–100% mesangial expansion and presence of sclerosis (extensive sclerosis with obliteration of the glomerular capillary tuft).

RNA sequencing

Total RNA from flash frozen cortical kidney sections was isolated using TRIzol Reagent (ThermoFisher) according to the manufacturer's protocol using kidney cortex tissue homogenates from 6-week-old rats (male $SS^{Xdh+/+}$ (N = 4), $SS^{Xdh+/-}$ (N = 4) and $SS^{Xdh-/-}$ (N = 4)) and sent to the Genomic Science and Precision Medicine Center (GSPMC) at the MCW for RNA sequencing. Total RNA was quantified by fluorometric methods and integrity was assessed with Fragment Analysis (Agilent Fragment Analyzer, Standard Sensitivity for RNA). RNA libraries were prepared according to the manufacturer's protocols utilizing Illumina's TruSeq Stranded mRNA library kit. Final assessment, quantification, and pooling of the RNAseq libraries were completed with qPCR (Kapa Library Quantification Kit, Kapa Biosystems) and DNA high sensitivity fragment analysis (Agilent, average size 310 bp). GSPMC completed sequencing on the NovaSeq6000 (Illumina) with paired-end 150 base pair reads generated at ~80 million total reads per sample. Sequencing reads were aligned to the rat Rnor_6.0.98 (Ensemble) transcriptome and processed through the MAPR-Seq Workflow (Kalari et al., 2014) with differential expression analysis completed using Bioconductor, edgeR v 3.8.6 software (Robinson et al., 2009). Genes with a false discovery rate (FDR) < 0.05 and an absolute fold change ≥1.5 were initially filtered and considered significantly differentially expressed.

Untargeted metabolomics

Snap-frozen kidney cortex tissue from 6-week-old male $SS^{Xdh+/+}$ (N = 5) and $SS^{Xdh-/-}$ (N = 4) rats were used for untargeted metabolomic analysis. The tissue was sent to the metabolomics core at the Mayo Clinic (Rochester, MN) (Trushina et al., 2013; Xyda et al., 2020). The tissue was homogenized after adding 10 μl/mg of PBS, and 50μl of the homogenate was deproteinized and centrifuged. The supernatants were used for analysis on a Quadrupole Time-of-Flight Mass Spectrometer (Agilent Technologies 6550 Q-TOF) coupled with an Ultra High-Pressure Liquid Chromatograph (1,290 Infinity UHPLC Agilent Technologies). Based on the method of acquiring profiling data (positive and negative electrospray ionization conditions) and Metabolite separation (two columns of differing polarity: hydrophilic interaction column (HILIC) and reversed-phase C18 column) the data were obtained in four modes. Initial data analysis was done using the R package MetaboanalystR. (FDR adjusted p value $\leq$ 0.05 and |fold change| $\geq$ 1.5).

Omics data visualization and pathway analysis

Datasets acquired by transcriptomics and metabolomics were analyzed using R packages (pheatmap, tidyverse, and ggplot2) and heatmaps were created. Further analysis was done using IPA software (QIAGEN Inc.). Using the lists generated by IPA further exploration of data and the schematic building was done manually using Microsoft office software.

QUANTIFICATION AND STATISTICAL ANALYSIS

Data are expressed as the ±SE of the mean, and data analysis for all protocols was performed blinded by an independent analyst. Data were tested for normality (Shapiro-Wilk) and equal variance (Levene's homogeneity test). Paired t-test was used to detect the statistical difference between two variables for the same

subject. For more than two groups of variables, the ANOVA test was used with corresponding Tukey or Dunnett post hoc analyses. Tukey or Dunnett multiple-comparisons adjustments were conducted only if the ANOVA F value was significant. p values of <0.05 (indicated *, #, ^) were considered significant. SigmaPlot 12.5 or GraphPad Prism 9 software was used to perform statistical tests.